Journal of Materials Chemistry A

Accepted Manuscript

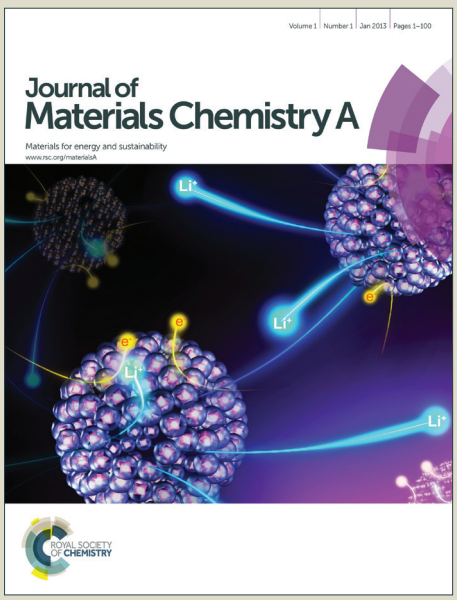

ROYAL SOCIETY OF CHEMISTRY

www.rsc.org/materialsA

Journal of

Materials Chemistry A

RSCPublishing

ARTICLE

Novel cathode-supported hollow fibers for light weight micro-tubular solid oxide fuel cells with active cathode functional layer

Cite this: DOI: 10.1039/x0xx00000x

Received ooth January 2012,
Accepted ooth January 2012

DOI: 10.1039/x0xx00000x

www.rsc.org/

Xiuxia Meng[a], Nai-Tao Yang[a],* Xun Gong[a], Yimei Yin[b], Zi-Feng Ma[b]*, Xiaoyao Tan[c], Zongping Shao[d], Shaomin Liu[d]*

Abstract: Micro-tubular SOFC has the potentials to become a light-weight portable auxiliary power unit for aircrafts or spacecrafts. In this work, a novel dual-layer ceramic hollow fiber for a cathode-supported micro-tubular solid oxide fuel cell (MT-SOFC) has been successfully developed via a co-spinning-sintering technique. The green cathode hollow fibers, in dual layer configuration, consisted of $La_{0.8}Sr_{0.2}MnO_{3-\delta}$ (LSM) main layer and LSM-Y_2O_3 stabilized ZrO_2 (YSZ) functional layer with increased three phase boundary length, are first prepared by co spinning, which are then sintered at around 1350°C to allow the creation of sufficient mechanical strength. Other cell components like the electrolyte (YSZ) and anode (NiO+YSZ) are then coated separately. The coated electrolyte film with a thickness around 27 μm is obtained by co-sintering of YSZ/LSM-YSZ/LSM in a sandwich structure. The porous LSM substrate functions as an oxygen-supplying and current collecting layer. The prepared MT-SOFC, tested with hydrogen as the fuel and air as the oxidant, delivers a maximum power density up to 475 mW•cm^{-2} at 850°C, which is much higher than the similar cell without a cathode functional layer.

1. Introduction

Fuel cells are very attractive for the conversion of chemical to electrical energy because of their high energy efficiencies thus conferring this novel power generation method with lower environmental impact[1-5]. Fuel cells are not restricted by the conventional thermodynamic limitations normally posed to these thermal plants as they are not heating engines for mechanical energy transfer. The fuel cell efficiencies, such as solid oxide fuel cells (SOFCs), are able to reach up to 80% if the waste-heat could be fully utilized[6]. If such fuel cell systems can be developed into cost-effective large scale applications, they may be able to replace these traditional thermal power plants, potentially lowering down the fuel consumption and emissions of CO_2 or other pollutants like SO_2 or NO_x. Among the various kinds of fuel cells, the polymer-electrolyte-membrane fuel cells (PEMFCs) and solid oxide fuel cells (SOFCs) currently receive the most attention[7-11]. PEMFCs are limited by the requirement of expensive catalyst like Pt and normally operated at lower temperatures. On the contrary, an SOFC is a solid-state device which can operate at much higher temperatures between 800 and 1000 °C[12-14]. The use of a solid electrolyte reduces corrosion in comparison to molten carbonate fuel cells while eliminating the water management problems possible in PEMFC[15,16]. Fuel choice for SOFC is very flexible with typical sources comprising of hydrogen, carbon monoxide, ammonia, methane, coal and other hydrocarbons. Planar and tubular geometries are the most common designs for SOFC. The tubular design has advantages over the planar counterpart with improved high temperature sealing and thermo-cycling behavior. The further reduction of the diameter of the tubular design leads to the microtubular SOFC (MT-SOFC), which promises faster operation of start up or shut down, higher volumetric power density, higher mass-transfer and heat-transfer efficiency[17,18]. For the certain required power output, the application of MT-SOFC features the reduced weight of fuel cell unit due to its high volumetric power density directly translating to a smaller cell unit size. Thus MT-SOFC has attracted intense research interest not only as a possible stationary heat power system but also as a light-weight portable auxiliary power unit in particular for aircrafts or spacecrafts.

Development of MT-SOFC is at very embryonic stage facing many challenges such as assembling all the components in the micro-tubular geometry. Luckily, recent progress in ceramic hollow fiber membranes facilitates its development. Typical SOFC components include electrolyte, anode and cathode plus interconnector and sealant via which the air and fuel flowing has been isolated into two different chambers. A few attempts have made to assemble the MT-SOFC by starting from the preparation of a hollow fiber support made from a single material of electrolyte, cathode or anode followed by the addition of other components via layer by layer using dip-coating or CVD techniques[19-21]. In some cases, in order to reduce the electrode resistance or increase the interface compatibility, an additional functional layer has to be sandwiched between the electrode and electrolyte; such practice makes the fabrication process more complex and uncertain. In this regard, a co-extrusion technique would definitely simplify the fabrication process by initially assembling two or more SOFC component layers simultaneously followed by sintering in one single step. This achievement is possible via a recent breakthrough technology-the preparation of dual-layer ceramic hollow fibers by the co-spinning and co-sintering technique in one step. On the basis of this method, several researchers have developed dual-layer structured anode/electrolyte hollow fiber supports for MT-SOFC applications[18,22,23]. Compared to the anode/electrolyte supported structures, the cathode-supported tubular SOFC can avoid the volume contraction and expansion stemming from anode redox reactions because of its thinner anode layer[19,24-26]. For instance, a stable long-term operation over 30,000 h using a cathode-supported tubular SOFC has been reported by Siemens Westinghouse Power[26]. Based on the co-spinning/sintering process, our group has successfully developed the dual-layer cathode/electrolyte hollow fibers for a cathode-supported MT-SOFC[27]. However, we observed that the power output of the resultant MT-SOFC was limited by the high cathodic resistance. In order to reduce such cathodic resistance and improve the MT-SOFC performance, an additional cathode functional layer (CFL) to increase the three-phase boundary (TPB) area will be added between the cathode and electrolyte, which is the main concern of this research. However, the addition of CFL via the conventional layer by layer in multistep method increases the process complexity.

In this work, we investigate the feasibility of using the phase-inversion assisted co-spinning technique to prepare the dual-layer cathode/CFL hollow fiber support and its application in MT-SOFC design. Among the SOFC studies, $La_{0.8}Sr_{0.2}MnO_{3-\delta}$ (LSM) and LSM-Y_2O_3 stabilized ZrO_2 (YSZ) have been respectively studied as the good cathode and CFL materials; and thus were chosen as the dual-layer hollow fiber material for demonstration. It should be noted that although the co-spinning/sintering method was reported previously and has certain versatility in application, the successful integration of two different ceramic phases in the single hollow fiber geometry from one sintering step still needs a lot of exploration to find the optimum spinning and sintering conditions to match each other to reach the best interface integration.

2 Experimental

2.1 Preparation of CFL/LSM dual-layer hollow fibers

All materials including $La_{0.8}Sr_{0.2}MnO_{3-\delta}$ (LSM), Y_2O_3 stabilized ZrO_2 (YSZ), polyether sulfone (PESf), N-methyl-pyrrolidone (NMP) and graphite pore former are the same as those have been reported previously[25]. The LSM-YSZ (60wt.% of LSM mixed with 40wt.% of YSZ) dope and LSM dope (15wt.% graphite) were co-spun simultaneously through a triple-orifice spinneret, passing through a 10 cm air gap, into a water coagulant bath. The spinning rates of the LSM-YSZ outer dope and the LSM internal dope were 1 mL min^{-1} and 10 mL min^{-1}, respectively; and the flow rate of internal coagulant (deionized water) was controlled at 14 mL min^{-1}. The spun precursors were immersed inside the external coagulation (water) bath for 24 hours to complete the solidification process. And then they were fully rinsed in clean water and cut into short pieces of 30 cm in length, and finally dried at room temperature. Finally, the green hollow fibers were calcined in the temperature range from 1300 to 1400°C in ambient non-flowing air for 10 h to obtain the CFL/cathode dual-layer hollow fibers. The parameters of the co-spinning process are shown in Table S1.

2.2 Preparation and testing of MT-SOFCs

The protocol to prepare the MT-SOFC based LSM-YSZ/LSM dual-layer hollow fiber is shown in Figure S1. The YSZ ink was dip-coated on the outer surface of the dry LSM-YSZ/LSM hollow fiber precursor[28], and co-sintered at temperatures from 1300 to 1400°C to fabricate the YSZ/CFL/LSM tri-layer membrane. Then NiO (60 wt %)-YSZ ink was coated on the outside of the electrolyte and sintered at 1200°C to form the anode of MT-SOFC[27].

MT-SOFC testing was carried out with a single cell setup described elsewhere[22, 27]. Prior to the measurement, the anode was first reduced with hydrogen at 700°C for 1 h. *I-V* & *I-P* data of the cells were collected using a DC Electronic Load (Keithley 2440-5A) at 700-850°C with hydrogen as fuel and air as oxidant. The flow rate of hydrogen and air were controlled at 40 and 90 mL•min^{-1}, respectively. Electrochemistry impedance resistances (EIS) of the cell under open circuit were measured by an electrochemistry workstation (Zahner IM6ex, Germany) in a frequency range of 1M to 0.01 Hz with a 10 mV perturbation.

2.3 Characterizations

The mechanical strength was measured using a three-point bending instrument (Instron Model 5544) with a crosshead speed of 0.5 mm•min^{-1}. The porosity of the hollow fibers was measured using a mercury porosimeter (Quantachome Instruments PM 60-6) with a mercury pressure of 138 kPa to 275.8MPa. The dimension of CFL/LSM dual-layer hollow fibers including the outer, inner diameters and wall thickness was determined by scanning electronic microscopy (SEM, FEI Sirion200, The Netherlands). Microstructures of the membranes and cells were also ascertained by SEM. The crystal phases of the prepared dual-layer hollow fibers were determined by X-ray diffraction (XRD, BRUKER D8 Advance, Germany) using Cu Kα radiation (λ= 0.15404 nm). Broken membrane was adhered in the XRD cell to expose the inner or outer surface to the X-ray. Continuous scan mode was used to collect 2θ data from 20° to 80° with a 0.02° sampling pitch and a 2° min^{-1} scan rate. The voltage and current of X-ray tube were set at 40 kV and

30mA, respectively. The elemental mapping images were investigated by the Energy Dispersive X-ray (EDX, Oxford Inca, UK).

3 Results and discussions

3.1 Microstructure and performance of CFL/LSM dual-layer hollow fibers

Figure 1 shows the SEM images of the dual-layer cathode supported hollow fibers sintered at different temperatures. In this hollow fiber geometry, the cathode -LSM layer is located at the inside part near the lumen and the cathode functional layer (CFL) (LSM+YSZ) is occupied the outer part. As can be seen, the asymmetric structure of the hollow fiber consists of a macro porous LSM support layer and a micro porous LSM-YSZ outer layer; the formation of such a porous morphology is largely dependent on the spinning and phase-inversion parameters. The macro porous LSM support is beneficial for oxidant transfer while the micro porous LSM-YSZ layer with larger surface area plays active cathode functional layer in favor of increasing TPBs for oxygen reduction. As the sintering temperature increased, both the LSM-YSZ and LSM layer were transferred to a denser structure (Figures 1 (a2-c2)), and the LSM and YSZ grains grew bigger (Figures 1 (a4-c4) & (a5-c5)). However, at 1400°C, the particles were over-densified leading to the formation of large crystals, which would possess less reaction activity (Figures 1 (c1-c5)). Our results indicate that the LSM-YSZ/LSM dual-layer hollow fibers should be sintered below 1400°C to avoid over-sintering of the cathode.

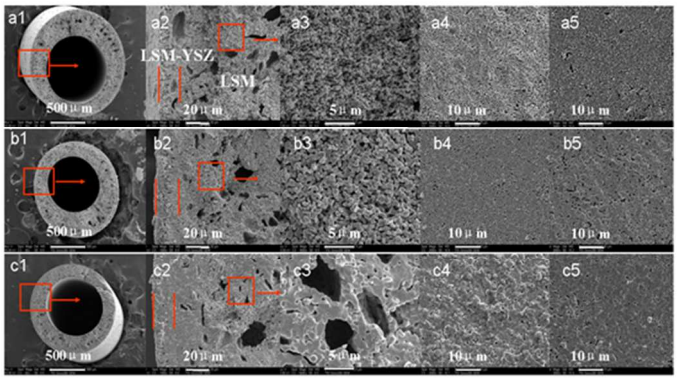

Figure 1 Microstructure of LSM-YSZ/LSM dual-layer hollow fiber membranes sintered at different temperatures. a-sintering at 1300℃; b- sintering at 1350℃; c- sintering at 1400℃; (1) cross-section; (2)Interface of LSM-YSZ/LSM; (3) Microstructure of LSM layer; (4) inner surface; and (5) outer surface.

Although a lower calcination temperature allows for a more porous cathode and CFL, beneficial for gas transfer and reaction, the sintering temperature cannot be too low as the good integration or the compatibility of the two layers and the mechanical strength of the resultant hollow fiber still requires a high sintering temperature. At 1350°C, the radial shrinkage of the CFL is slightly higher than the LSM layer as shown in Figure 2, which is the reason that the outer CFL can tightly surround the inner hollow LSM layer. The good integration of the two layers fulfilled at this temperature is favorable to decrease cathode resistance and stabilize multilayer structure. Meanwhile, the porosity of dual-layer hollow fibers is 37% (Figure 3), sufficient for the rapid transport of oxidant in cathode. Such achievement is heavily relying on the optimized dope composition, the spinning and sintering conditions (Table S1). A lot of other compositions and conditions had been attempted but all of which failed.

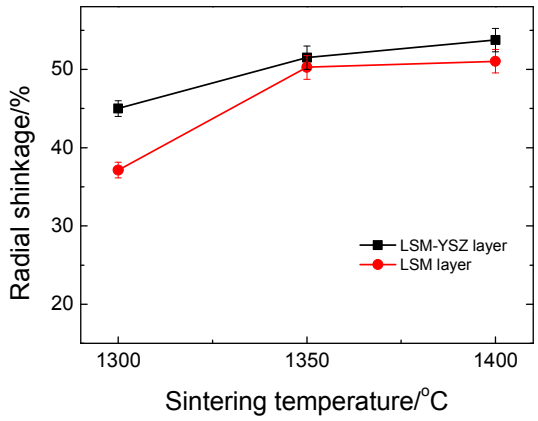

Figure 2 Radial shrinkage of LSM & LSM-YSZ layer as a function of sintering temperature.

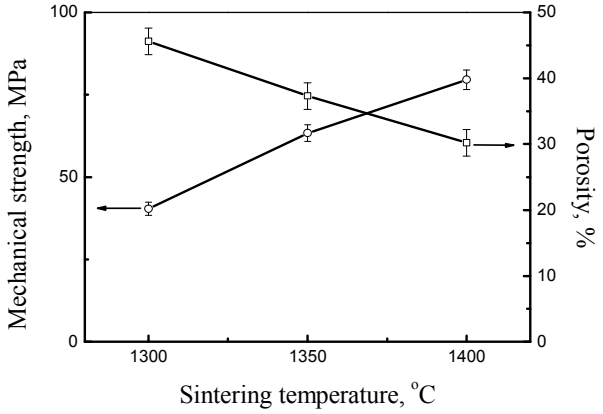

Figure 3 Porosity and mechanical strength of the dual-layer LSM-YSZ/LSM hollow fiber at different sintering temperature.

To support other SOFC components such as electrolyte and anode, the dual-layer hollow fiber should possess a certain high mechanical strength. Sintered at 1350°C, the bending strength is about 65 MPa (Figure 3), which is sufficiently robust to be routinely handled to fabricate the MT-SOFC as a cathode support. Therefore, the temperature of 1350°C is the optimum sintering parameter to calcine LSM-YSZ/LSM dual-layer hollow fibers.

3.2 Microstructure of YSZ/CFL/LSM tri-layer membrane

Figure 4 shows the SEM of the YSZ/CFL/LSM tri-layer membrane sintered at 1350°C. The YSZ layer was coated outside the CFL/LSM hollow fiber. The outside diameter and inside diameter of the tri-layer membrane are 1.3 and 0.8 mm, respectively. The magnified part of the hollow fiber cross section in Figure 4 (b) clearly displays three different layers

(marked by white lines) in sequence of YSZ/LSM-YSZ/LSM with thickness of 27, 20, and 190 μm, respectively. A careful inspection of these interfaces between these cell components illustrates that they were integrated very well without any sign of delamination. The prerequisite of such achievement is the successful preparation of the high quality substrate of LSM-YSZ/LSM dual-layer hollow fiber, leading to an excellent match of thermal and mechanical capability between the YSZ and LSM-YSZ layer rather than the direct contact between YSZ and LSM.

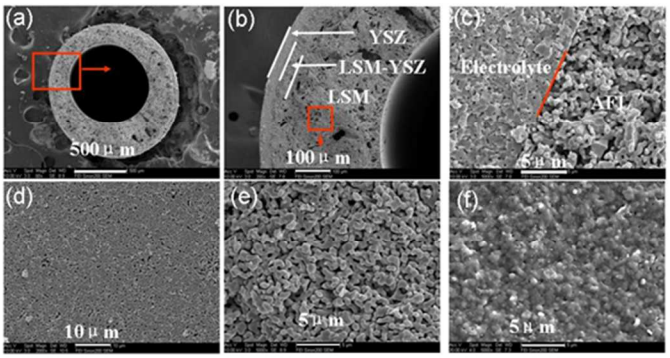

Figure 4 Microstructure of the YSZ/CFL/LSM tri-layer hollow fibers sintered at 1350℃. (a) over-view; (b) cross-section; (c) interface of YSZ/CFL; (d) inner surface; (e) LSM layer; (f) outer surface.

Although some small pores still remain in the electrolyte, pure YSZ layer, at 1350 °C (Figure 4(c) & (f)), there is no connected porosity for fuel molecular to pass through. In contrast, CFL/LSM support layers (Figure 4 (d) & (e)) are still in porous structure beneficial for gas transport and current collection, lowering the ohmic resistance and concentration polarization of MT-SOFCs. The intermediate layer of CFL (LSM-YSZ) between electrolyte and LSM is very thin, and its overall porosity is not as high as the pure LSM support. The porous structure of LSM-YSZ layer helps to maintain the high three-phase boundary (TPB) area, favoring a decrease in the activation polarization resistance.

Localized voltage anomalies were observed by other researchers due to the loss of electrical contact of the adjacent cell bundles during the operation process of the cathode-supported tubular SOFC stack developed by Siemens Westinghouse[29]. Therefore, during the co-sintering of the YSZ/CFL/LSM tri-layers, the elemental diffusion between different layers should be avoided as much as possible since it may lead to a similar short circuit phenomenon inside the electrolyte and loss of cell efficiency. Elemental mapping result of La, Mn and Zr on the cross-section of the YSZ/CFL/LSM tri-layer membrane is displayed in Figure 5.

As can be seen, the cathode elements such as La and Mn are continuously distribute in the CFL and LSM support layers, but could not be detected in the electrolyte layer. This indicates that the two elements did not diffuse into YSZ layer during the co-sintering process, eliminating the possibility of electronic short circuit from CFL to the anode. Furthermore, the element of Zr is continuously distributed in CFL and electrolyte layers (Figure 5 (c)), a good integration of the electrolyte with the cathode and the extended TPBs from electrolyte/cathode interface to the interior of cathode.

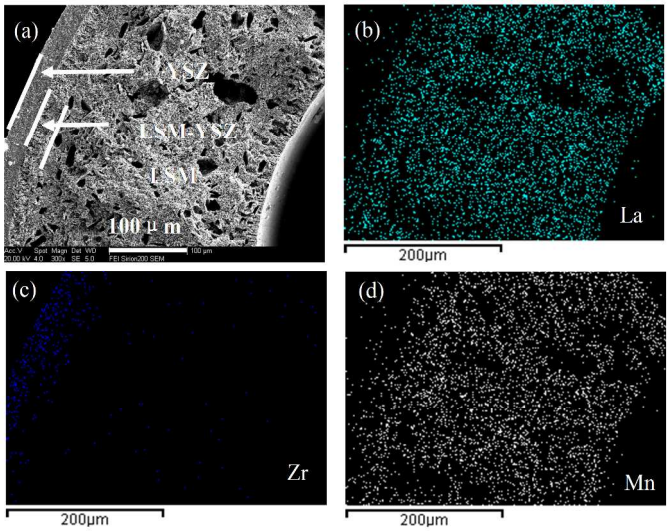

Figure 5 Microstructure and X-ray energy dispersive spectrometry (EDX) analysis of YSZ/CFL/LSM tri-layer membran e sintered at 1350 °C, (a) cross section, (b) La mapping; (c) Zr mapping, (d) Mn mapping.

Figure 6 describes the X-ray diffraction (XRD) patterns of the YSZ/CFL/LSM tri-layer membrane performed on the inner cathode surface and the outer electrolyte surface. Only a pure YSZ or LSM phase can be detected from the outer surface or from the inner surface, respectively, which is consistent with the observation in Figure 5. This further confirms that the LSM phase was hardly diffused into the electrolyte layer during the co-sintering process.

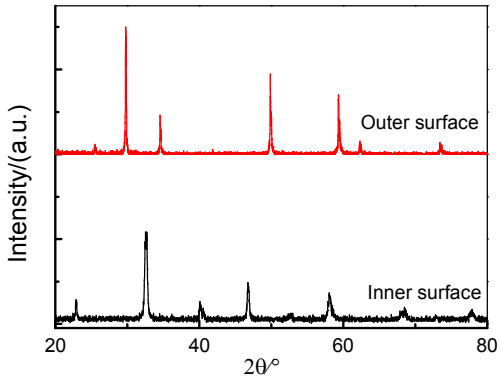

Figure 6 XRD of inner surface and outer surface of the YSZ/CFL/LSM tri-layer membrane.

3.3 Performance of the cathode-supported MT-SOFCs

A NiO-YSZ anode layer was dip-coated on the outer surface of the 1350°C-sintered YSZ/CFL/LSM membrane to form micro-tubular fuel cells. Figure 7 depicts the cross-sectional SEM images of a fully assembled cell based on the NiO-YSZ/YSZ/CFL/LSM tetro-layer membrane sintered at 1350 °C. As seen, the coated anode is around 5 μm in thickness and integrates well with the substrate.

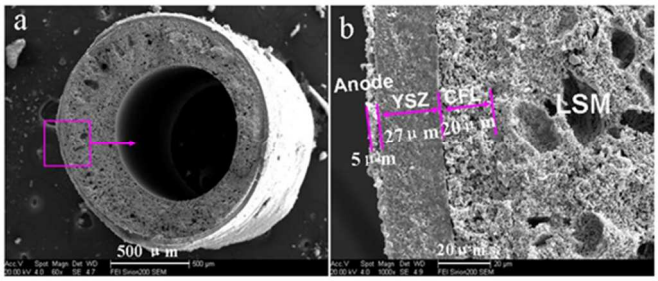

Figure 7 Microstructure of dual-layer cathode-supported MT-SOFC. (a) cross-section; (b) anode/electrolyte/CFL/LSM interface.

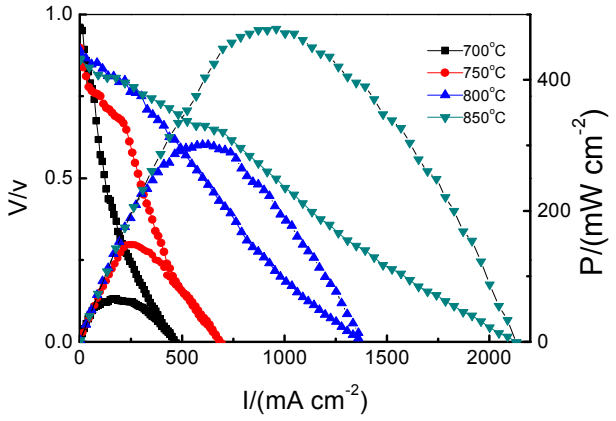

Figure 8 Output of MT-SOFC based on the LSM-YSZ/LSM dual-layer hollow fibers (H_2 feed flow rate = 40 mL min^{-1}; air feed flow rate = 90 mL min^{-1}).

Figure 8 shows the *I-P* & *I-V* curves of a prepared cathode-supported MT-SOFC using H_2 as fuel and air as oxidant operated at 700-850 °C. From Figure 8, the open-circuit voltages (OCVs) vary from 0.95 to 0.84 V, a bit lower than the theoretical value, but the result is still promising. Its peak power densities could reach 65, 148, 301 and 475 mW cm^{-2}, respectively, at 700, 750, 800 and 850 °C, higher than the corresponding values of our previous cathode-supported cell without the CFL[27]. This performance enhancement can be attributed to the decreasing polarization resistance which is induced by the insertion of CFL and the implementation of better current collecting layer. Figure 9 exhibits the EIS of the prepared cell operated under OCVs. The total resistance (*R*t) and ohmic resistance (*R*o), corresponding to the low frequency intercept and the high frequency intercept, respectively, can be obtained from the impedance spectra. The polarization resistance (*R*p) of the cell can be obtained by subtracting Ro from Rt. The *R*p dominated the total cell resistance at the low temperatures and the effect of the ohmic resistance on the total cell resistance increased with the increase of temperature. For example, the ohmic resistance and polarization resistance of the cell were 1.71 and 9.2 Ω cm^2 at 700 °C, and 0.45 and 0.82 Ω cm^2 at 850 °C, respectively, significantly lower than the cathode-supported cell, due to the increase of reaction sites induced by CFL insertion[27]. The performance of the single cell was mainly controlled by the polarization resistance at low temperature, but jointly controlled by both polarization and ohmic resistance at high temperatures. Therefore, the polarization resistance is still a key obstacle to enhance output of the cathode-supported MT-SOFC. How to decrease the polarization resistance by optimizing the sintering temperature and the cell component thickness is still going in our lab. The cathode infiltration by some electro-catalysts with highly active oxygen activation is an interesting alternative to improve the performance of the cells[30]. The results of the MT-SOFC further performance improvement will be reported in the future.

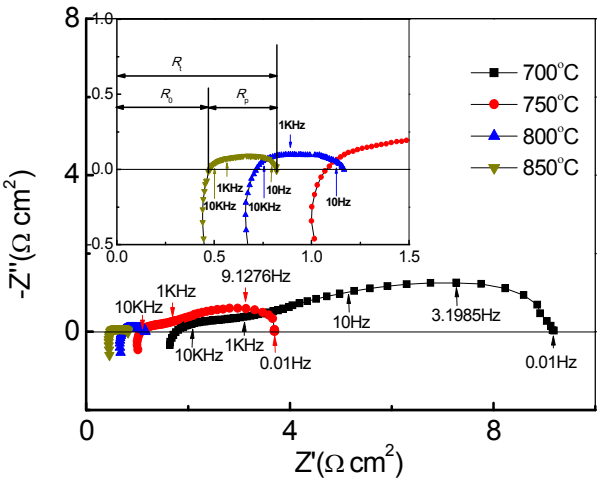

Figure 9 EIS of MT-SOFC at different temperatures under open circuit condition.

4 Conclusions

A novel cathode supported hollow fiber with additional cathode functional layer has been successfully developed in a single step via a combined co-spinning-sintering method. The developed dual-layered hollow fiber has potentials in achieving the light-weight micro-tubular solid oxide fuel cells. To form the cathode-supported MT-SOFC, the electrolyte (YSZ) film and anode (NiO-YSZ) were separately coated and heat-treated at 1350°C. Compared to the previously developed cathode supported MT-SOFC without additional cathode functional layer, the present dual-layered MT-SOFC performed very favorably by delivering a much higher OCVs and peak power densities. The cathode functional layer increases the reaction efficiency by providing more three-phase boundary area. The peak power density is up to 475 mW cm^{-2}, operated at 850oC, using hydrogen as fuel and air as oxidant.

Acknowledgement

The authors gratefully acknowledge the research funding provided by the National Natural Science Foundation of China (21376143, 21176146 and 21173147), and the Natural Science Foundation of Shandong Province (ZR2013BM010). Dr. Shao

and Dr. Liu acknowledge the support from Australian Research Council Future Fellowship.

Notes and references

[a] School of Chemical Engineering, Shandong University of Technology, Zibo 255049, China
[b] Institute of Electrochemical and Energy Technology, Department of Chemical Engineering, Shanghai Jiao Tong University, Shanghai 200240, China
[c] Department of Chemical Engineering, Tianjin Polytechnic University, Tianjin300387, China
[d] Department of Chemical Engineering, Curtin University, Perth, WA 6845, Australia
*Corresponding author Email address: naitaoyang@126.com; zfma@sjtu.edu.cn; shaomin.liu@curtin.edu.au
Telephones: +86-533-2786292; +61-08-92669056
Fax:+86-533-2786292; +61-08-92662681

References

1. Z. Shao, S. M. Haile, J. Ahn, P. D. Ronney, Z. Zhan and S. A. Barnett, Nature, 2005, 435, 795-798.
2. Y. Jee, G. Y. Cho, J. An, H.-R. Kim, J.-W. Son, J.-H. Lee, F. B. Prinz, M. H. Lee and S. W. Cha, Journal of Power Sources, 2014, 253, 114-122.
3. S. B. Weber, T. Grande, G. W. Scherer and M.-A. Einarsrud, Journal of the American Ceramic Society, 2013, 96, 420-428.
4. V. Sariboğa and F. Öksüzömer, Applied Energy, 2012, 93, 707-721.
5. P. Vijay, M. O. Tadé and R. Datta, Industrial & Engineering Chemistry Research, 2010, 50, 1439-1452.
6. P. Vijay, M. O. Tade and R. Datta, Ind. Eng. Chem. Res., 2011, 50, 1439-1452.
7. F. Dong, Y. Chen, R. Ran, M. O. Tade, S. Liu and Z. Shao, J. Mater. Chem. A, 1 (2013) 9781-9791.
8. Y. Nabae, Y. Kuang, M. Chokai, T. Ichihara, A. Isoda, T. Hayakawa, T. Aoki, J. Mater. Chem. A, 2014,2, 11561-11564.
9. J. K. Koh, Y. K. Jeon, Y. Cho, J. H. Kim and Y-G. Shul, J. Mater. Chem. A, 2014,2, 8652-8659.
10. P. Divya and S. Ramaprabhu, J. Mater. Chem. A, 2014,2, 4912-4918.
11. S. Wang, C. Zhao, W. Ma, N. Zhang, Y. Zhang, G. Zhang, Z. Liu and H. Na, J. Mater. Chem. A, 2013,1, 621-629.
12. X.-F. Ye, S. R. Wang, J. Zhou, F. R. Zeng, H. W. Nie and T. L. Wen, Journal of Power Sources, 2011, 196, 5499-5502.
13. T. Suzuki, S. Sugihara, T. Yamaguchi, H. Sumi, K. Hamamoto and Y. Fujishiro, Electrochemistry Communications, 2011, 13, 959-962.
14. D. Ding, X. Li, S. Y. Lai, K. Gerdes and M. Liu, Energy & Environmental Science, 2014, 7, 552-575.
15. Z. Zhan and S. A. Barnett, Science, 2005, 308, 844-847.
16. S. P. Jiang, International Journal of Hydrogen Energy, 2012, 37, 449-470.
17. M. A. Laguna-Bercero, A. R. Hanifi, H. Monzón,a J. Cunningham, T. H. Etsell and P. Sarkar, J. Mater. Chem. A, 2014,2, 9764-9770.
18. M. H. D. Othman, N. Droushiotis, Z. Wu, G. Kelsall and K. Li, Advanced Materials, 2011, 23, 2480-2483.
19. C. Zhao, R. Liu, S. Wang, Z. Wang, J. Qian and T. Wen, Journal of Power Sources, 2009, 192, 552-555.
20. T. Yamaguchi, S. Shimizu, T. Suzuki, Y. Fujishiro and M. Awano, Electrochemistry Communications, 2008, 10, 1381-1383.
21. T. Yamaguchi, S. Shimizu, T. Suzuki, Y. Fujishiro and M. Awano, Journal of The Electrochemical Society, 2008, 155, B423-B426.
22. X. Meng, X. Gong, Y. Yin, N.-T. Yang, X. Tan and Z.-F. Ma, International Journal of Hydrogen Energy, 2013, 38, 6700-6788.
23. M. H. D. Othman, Z. Wu, N. Droushiotis, U. Doraswami, G. Kelsall and K. Li, Journal of Membrane Science, 2010, 351, 196-204.
24. R. Campana, R. I. Merino, A. Larrea, I. Villarreal and V. M. Orera, Journal of Power Sources, 2009, 192, 120-125.
25. T. Suzuki, Y. Funahashi, Z. Hasan, T. Yamaguchi, Y. Fujishiro and M. Awano, Electrochemistry Communications, 2008, 10, 1563-1566.
26. K. Huang and S. C. Singhal, Journal of Power Sources, 2013, 237, 84-97.
27. X. Meng, X. Gong, N. Yang, X. Tan, Y. Yin and Z.-F. Ma, Journal of Power Sources, 2013, 237, 277-284.
28. N.-T. Yang, X. Tan, X.-X. Meng, Y. Yin and Z.-F. Ma, ECS Transactions, 2009, 25, 881-888.
29. R. A. George, Journal of Power Sources, 86, 134-139.
30. José M. Serra and Vicente B. Vert, ChemSusChem, 2009, 2 957 -961.

